PLOS ONE

RESEARCH ARTICLE

Performance analysis of dual-hop mixed RF-FSO systems combined with NOMA

Tran Cong Hung[1], Tan N. Nguyen[2,3], N. H. K. Nhan[3]*, Anh-Tu Le[2], Pham Ngoc Son[4], Thu-Ha Thi Pham[5], Miroslav Voznak[2]

1 Dean of School of Computer Science & Engineering, The SaiGon Internaltional University, Ho Chi Minh City, Vietnam, **2** Faculty of Electrical Engineering and Computer Science, VSB-Technical University of Ostrava, Ostrava, Czechia, **3** Communication and Signal Processing Research Group, Faculty of Electrical and Electronics Engineering, Ton Duc Thang University, Ho Chi Minh City, Vietnam, **4** Faculty of Electrical and Electronics Engineering, Ho Chi Minh City University of Technology and Education, Thu Duc City, Ho Chi Minh City, Vietnam, **5** Faculty of Electrical and Electronics Engineering, Ton Duc Thang University, Ho Chi Minh City, Vietnam

* nguyenhuukhanhnhan@tdtu.edu.vn

Citation: Hung TC, Nguyen TN, Nhan NHK, Le A-T, Son PN, Pham T-HT, et al. (2024) Performance analysis of dual-hop mixed RF-FSO systems combined with NOMA. PLoS ONE 19(12): e0315123. https://doi.org/10.1371/journal.pone.0315123

Editor: Rahat Ullah, Nanjing University of Information Science and technology, Nanjing, China., CHINA

Received: July 15, 2024

Accepted: November 20, 2024

Published: December 20, 2024

Peer Review History: PLOS recognizes the benefits of transparency in the peer review process; therefore, we enable the publication of all of the content of peer review and author responses alongside final, published articles. The editorial history of this article is available here: https://doi.org/10.1371/journal.pone.0315123

Data Availability Statement: All relevant data are within the manuscript and its Supporting information files.

Abstract

This paper investigates the performance of hybrid radio frequency/free space optical (RF/FSO) systems combined with non-orthogonal multiple access communications technology. We examine a scenario where the source and destination are separated by a large distance, with no direct link between them. The relay, denoted R, operates using the decode-and-forward (DF) protocol. Under the DF relaying scheme, the relay employs successive interference cancellation (SIC). In this setup, the FSO link from the source to the relay follows a Gamma-Gamma distribution, while the RF link from the relay to multiple users follow a Nakagami-*m* distribution. Based on this system model, we analyze the outage probability (OP). Our findings indicate a direct relationship between SIC and OP performance: the higher the SIC capability, the more effective the system. In addition, the system's performance is dependent on the parameters of the FSO channel. Finally, Monte Carlo simulations are presented to further validate our framework and findings.

1 Introduction

One of the most significant breakthroughs in the history of telecommunications was the invention of wireless communication. The proliferation and prevalence of wireless devices have exceeded expectations from a few decades ago and are predicted to continue growing at an exponential rate. Radio frequency (RF) technology has dominated wireless communication systems, occupying both licensed and unlicensed spectrums, in a wide variety of contexts [1, 2]. This dominance has led to widespread adoption and the existence of a large number of RF devices. However, several issues underlie the use of the RF band, including limited capacity, high costs of licensed spectrum technologies, and interference from unlicensed spectrum technologies. With the number of consumer devices growing exponentially, researchers are exploring novel wireless communication methods. It is essential to evaluate additional frequency bands in the electromagnetic spectrum for data transfer since the demand for constant

Funding: This research is funded by the European Union within the REFRESH project - Research Excellence For Region Sustainability and High-tech Industries ID No. CZ.10.03.01/00/22 003/0000048 of the European Just Transition Fund and by the Ministry of Education, Youth and Sports of the Czech Republic (MEYS CZ) through the project SGS ID No. SP 061/2024 conducted by VSB - Technical University of Ostrava.

Competing interests: The authors have declared that no competing interests exist.

communication availability exceeds the RF spectrum's capacity. In this context, free-space optical (FSO) communication systems have drawn much interest from both academic and industry communities for their ease of implementation, low power consumption, high data rates and bandwidth, and free spectrum licensing [3–7]. Compared to traditional RF communications, FSO communications offer higher throughput, the use of unlicensed spectrums, cost-effectiveness, and other advantages. FSO systems represent a promising solution for various communications scenarios, which include backhaul/fronthaul link for cellular systems, aerial/drone-assisted wireless emergency communications for disaster recovery, and optical communications for space exploration [6, 8, 10].

Since mixed FSO-RF networks can benefit from both the broadcasting nature and wide coverage area of the RF technique as well as the high channel capacity, license-free operation, and enhanced security of the FSO technique, they have attracted a lot of interest. In an FSO-RF system, a cooperative relay is used as an intermediary to transfer signals from the transmitter to the receiver. Relay strategies are divided into two categories: protocols for amplify-and-forward (AF) relaying and decode-and-forward (DF) relaying [11]. Various fading models are also employed in the FSO and RF channels of hybrid FSO-RF relaying systems. The FSO link can function according to Gamma-Gamma [12–16] or exponentiated Weibull distributions [17, 18], among others. In contrast, the RF link can operate under Rayleigh [12, 13], Nakagami-m [14, 17, 19], generalized K–μ [18], and K distributions [20]. For example, the hybrid FSO-RF system described in [12], applies RF and FSO link defined according to the Rayleigh and Gamma-Gamma distributions, respectively, and uses an AF relay. In another study [17], both fixed-gain and variable-gain relay schemes are examined, using an RF link modeled according to the Nakagami-m distribution and an FSO link under exponentiated Weibull fading. A dual-hop hybrid FSO-RF system characterized by RF and FSO link that follow Nakagami-m and double generalized Gamma distributions, respectively, is described in [19]. Similarly, an asymmetric dual-hop AF relaying system employing RF and FSO link under Nakagami-m and Gamma-Gamma fading, respectively, is discussed in [14].

Non-orthogonal multiple access (NOMA) also leverages non-orthogonal resource allocation to enable a high number of users access the network, in contrast to traditional orthogonal multiple access (OMA) technologies. Recently, NOMA has garnered much interest as an essential technology for 5G wireless communication networks [21–25]. To ensure fairness among users, NOMA assigns lower power levels to users with stronger channel gains and higher power levels to users with weaker channel gains [26, 27]. These signals are then superposed at the source. Academic and industrial research have also demonstrated that NOMA can effectively support vast connectivity in addition to its increased spectral efficiency. This capability is crucial for supporting the Internet of Things (IoT) features in the forthcoming 5G Next networks [28–30]. Due to NOMA's interoperability with various communication technologies, it can be seamlessly integrated into both current and future wireless systems. For instance, it has been demonstrated that NOMA is compatible with traditional OMA methods such as orthogonal frequency division multiple access (OFDMA) and time division multiple access (TDMA) [31]. NOMA has also been incorporated into the next digital TV standard, known as layered division multiplexing [32], which enhances the spectral efficiency of TV broadcasting by superimposing numerous data streams. Recent research has also explored the use of NOMA with unmanned aerial vehicle (UAV) systems [33, 34] and in satellite architectures [35, 36]. The application of multiple intelligent reflecting surfaces (IRSs) with distinct phase shifts to support NOMA networks has also been examined [37, 38]. These aforementioned instances highlight NOMA's enormous potential not only for 5G networks but also for various current and future wireless systems.

1.1 Related work

Exploiting the advantages of both the high data rates facilitated by FSO systems and the high spectral efficiency introduced by NOMA serves as the primary motivation for combining FSO and NOMA. Another reason is that NOMA typically operates well in situations where the power received from various transmitters varies significantly [27]. This condition is often encountered in FSO systems because adverse weather conditions, such as haze and fog, result in higher path loss for FSO link compared to RF lines. However, the combination of FSO and NOMA has only recently been explored in the literature [39–41]. In [39], the authors consider employing NOMA for the FSO backhauling system, which consists of two base stations and one central unit. Another study [40] examines a multi point-to-point system consisting of K users and a central node using NOMA over an FSO channel. In [41], the authors investigate a low-altitude platform (LAP)-aided dual-hop relaying system that combines NOMA and FSO communications technology.

In addition, the incorporation of NOMA with mixed FSO-RF networks to achieve better communication performance [42–47]. A two-hop uplink NOMA RF-FSO network was investigated in [42] in order to meet the high throughput requirements for the backhaul connection. The closed-form formulation of OP and ergodic channel capacity under various interference situations was also provided. The subject of the combined optimization of power allocation and harvesting time was further investigated in [43] when the analytical expressions of OP and throughput were taken into consideration in the context of an energy harvesting enabled mixed FSO-RF network. By including NOMA into both the FSO and RF connections, the authors of [44] suggested a down-link FSO-RF network and determined the closed-form expression of OP for every user. The analytical formulation of OP was introduced in [45], taking into account that the RF channel has a Rayleigh distribution and the FSO channel has an M-distribution. [46] provided the analytical and asymptotic formulas of secrecy OP (SOP) for an FSORF system with NOMA while accounting for the imperfect channel state information. For a NOMA-based hybrid RF-UWOC system, the asymptotic formulations of ergodic capacity and the closed-form formulas of OP were provided in [47].

1.2 Contributions

Based on the above-mentioned issues, it is highly intriguing and promising to research the FSO-RF cooperation with NOMA. In this paper, we consider a data transmission protocol where a relay is available between the source and multiple destinations to investigate the effect of OP. Table 1 shows the comparison between our work and related papers and the key notations are used in this paper, as shown in Table 2. Our main contributions are as follows:

- A proposed dual-hop mixed RF/FSO system that includes both RF and FSO link. In this system, the FSO link, which connects the source to the relay, follows a doubly generalized

Table 1. The comparison of our work and the previous works.

Ref./Prop.	Dual-hop FSO-RF	Nakagami-*m* fading	NOMA	OP	Asymptotic	Stochastic Geometry
[48]	✓	✓	✓	✓	X	X
[49]	✓	✓	✓	✓	✓	X
[50]	✓	✓	X	✓	X	X
[51]	X	X	X	✓	X	✓
[52]	✓	X	X	✓	✓	X
Our study	✓	✓	✓	✓	✓	✓

https://doi.org/10.1371/journal.pone.0315123.t001

Table 2. Main parameter notation.

Symbol	Notation	Symbol	Notation
x_i	Signal at User i, $i \in \{1, 2\}$	a_i	Power allocation coefficients at User i
R^i_{th}	Target rate at User i	γ^i_{th}	Threshold rate of User i
P_S	Transmit power at Source	P_R	Transmit power at Relay
d_1	Distance from R to near user	d_2	Distance from R to far user
L	Distance from S to R	δ	Path loss exponent
h_0	Channel gain from S to R	h_1	Channel gain from R to near user
h_2	Channel gain from R to far user	$\mathcal{CN}(u, \sigma^2)$	Complex Gaussian random variable
$f_X(\cdot)$	Probability density function (PDF) of X	$F_X(\cdot)$	Cumulative distribution function (CDF) of X
$\Pr(\cdot)$	Probability operator	$\mathbb{E}\{\cdot\}$	Expectation operator
$\lvert\cdot\rvert$	Absolute value of a complex number	$\Gamma(\cdot)$	Gamma function
$\Gamma(\cdot, \cdot)$	Upper incomplete Gamma function	$\gamma(\cdot, \cdot)$	Lowe incomplete Gamma function
$K_q(\cdot)$	Bessel function of the second kind	$G^{m,n}_{p,q}(.)$	Meijer G-function

https://doi.org/10.1371/journal.pone.0315123.t002

Gamma distribution. The RF link, connecting the relay to multiple users, follows the Nakagami-*m* distribution. The cooperative relay, functioning as an intermediary to transmit signals from the transmitter to the receiver, employs DF relaying. We examine the signal-to-interference-plus-noise ratio (SINR) for both the FSO and RF link when relay R uses successive interference cancellation (SIC), in addition to the SINR when relay R applies imperfect SIC (ipSIC).

- To ensure the secure performance of the proposed system, we derive the OP expressions for both near and far users. Notably, we investigate the outages in the high-SNR regime. Analysis and simulation results evaluate the impacts of key parameters on performance.

1.3 Overview

Following the introduction in Section 1, Section 2 presents the system model of FSO/RF cooperative NOMA and the channel characteristics of FSO and RF. In Section 3, we obtain the statistical properties of the FSO/RF link. In Section 4, we derive the analytical expressions for the OP for three cases: near users, far users, and both near and far users under a high SNR regime. Section 5 provides numerical and simulation results to verify the theoretical analyses. Section 6 concludes the paper with a summary of its main findings and contributions.

2 System model and channel characteristics

In this paper, we consier the FSO/RF Cooperative NOMA system model with a source (S), a relay (R), and two users as in Fig 1. It is assumed that R operates in half-duplex mode and that the channel state information (CSI) is perfect at each terminal to detect the signal. The communications from S to R and R to D_i, $i \in \{1, 2\}$ therefore occupy two-time slots. In the first time slot, by applying NOMA principle, S using NOMA signaling $\sqrt{a_1 P_S}x_1 + \sqrt{a_2 P_S}x_2$ to transmits to R through the FSO link, where P_S is the transmission power at S, x_1 and x_2 are the unit-power data symbols, a_1 and a_2, $a_2 > a_1$ are the corresponding power allocation coefficients. The signal received at the R is therefore expressed as

$$Y_R = h_0(\sqrt{a_1 P_S}x_1 + \sqrt{a_2 P_S}x_2) + n_R, \tag{1}$$

where n_R is the additive Gaussian noise at the relay in which $n_i \sim \mathcal{CN}(0, \sigma^2)$.

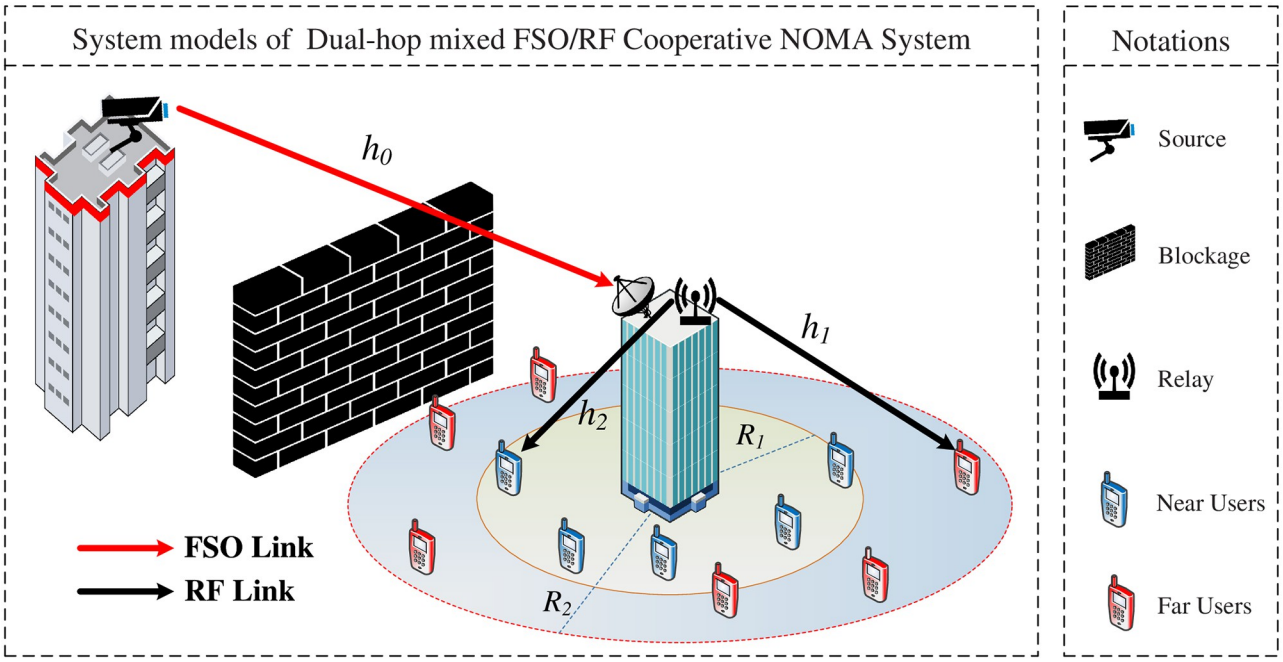

Fig 1. FSO/RF cooperative NOMA system model.

https://doi.org/10.1371/journal.pone.0315123.g001

2.1 FSO link

Using the NOMA protocol, R decodes the information from S in x_2 by considering x_1 as an interference signal. The received SINR to identify x_2 at R is therefore given by

$$\begin{aligned}\gamma_{R,x_2}^{SIC} &= \frac{a_2 P_S |h_0|^2}{a_1 P_S |h_0|^2 + \sigma^2} \\ &= \frac{a_2 \rho |h_0|^2}{a_1 \rho |h_0|^2 + 1},\end{aligned} \tag{2}$$

where $\rho = P_S/\sigma^2$ denotes the transmit signal-to-noise ratio (SNR). Note that x_1 and x_2 are normalized unity power signals, i.e, $\mathbb{E}\{x_1^2\} = \mathbb{E}\{x_2^2\} = 1$.

After performing SIC at R to identify x_2, the received SINR at R to detect x_1 in the case of imperfect SIC is expressed as

$$\gamma_{R,x_1}^{ipSIC} = \frac{a_1 \rho |h_0|^2}{\chi a_2 \rho |h_0|^2 + 1}. \tag{3}$$

where χ, $0 \leq \chi \leq 1$, representing the efficiency of SIC for x_2 at R. The cases $\chi = 0$ and $\chi = 1$ correspond to perfect SIC (pSIC) and imperfect SIC (ipSIC) in [53], respectively.

2.2 RF link

After receiving Y_R, the relay decodes and transmits the signal to end users via Nakagami-m fading RF channel. By similarly applying NOMA principle in FSO link, R transmit the NOMA signaling $\sqrt{a_1 P_R} x_1 + \sqrt{a_2 P_R} x_2$ to user D_i. Thus, the signals received at D_i is therefore expressed

as

$$Y_{D_u} = \frac{h_u}{\sqrt{d_u^{\delta}}}(\sqrt{a_1 P_R}x_1 + \sqrt{a_2 P_R}x_2) + n_u \quad , u \in \{1, 2\} \tag{4}$$

where P_R is the normalized transmission power at R, d_u is the distance between R and D_u, and δ is the path-loss exponent.

Using the NOMA protocol, since the user with the highest received signal strength, D_1, applies SIC, the SINRs required to perform SIC for x_1 and x_2 at D_1 are given by

$$\gamma_{1,x_2}^{SIC} = \frac{a_2\rho|h_1|^2}{a_1\rho|h_1|^2 + d_1^{\delta}}, \tag{5}$$

$$\gamma_{1,x_1}^{ipSIC} = \frac{a_1\rho|h_1|^2}{\chi a_2\rho|h_1|^2 + d_1^{\delta}}. \tag{6}$$

In contrast, D_2 decodes its intended signal x_2 by treating x_1 as interference. Consequently, the SINR at D_2 is

$$\gamma_{2,x_2} = \frac{a_2\rho|h_2|^2}{a_1\rho|h_2|^2 + d_2^{\delta}}. \tag{7}$$

3 Performance analysis

In an investigation of the system performance, we first obtain the statistical property of the FSO/RF link.

3.1 Channel model

3.1.1 Fading statistics of the FSO channel. Let $\gamma_0 \triangleq |h_0|^2$ be a K_G distributed random variables (RV) with three gamma-gamma parameters that were obtained from its square. This PDF is provided by [54, Eq. (1)]:

$$f_{\gamma_0}(x; \alpha, \beta, \Omega_0) = \frac{2(\alpha\beta)^{\frac{\alpha+\beta}{2}} x^{\frac{\alpha+\beta}{2}-1}}{\Gamma(\alpha)\Gamma(\beta)\Omega_0^{\frac{\alpha+\beta}{2}}} K_{\alpha-\beta}\left(2\sqrt{\frac{\alpha\beta}{\Omega_0}x}\right), \tag{8}$$

where $\alpha \geq 0$ and $\beta \geq 0$ are the factors that determine the shaping of the small-scale and large-scale eddies in the scattering environment, and Ω_0 relates to the mean as $\mathbb{E}[\gamma_0] = \Omega_0$, in which $\mathbb{E}[\cdot]$ denotes expectation. The two effective numbers, α and β, relate to the atmospheric conditions and are expressed as [55]

$$\alpha = \left(\exp\left[\frac{0.49\sigma_0^2}{(1 + 0.18d_0^2 + 0.56\sigma_0^{12/5})^{7/6}}\right] - 1\right)^{-1}, \tag{9}$$

$$\beta = \left(\exp\left[\frac{0.51\sigma_0^2(1 + 0.69\sigma_0^{12/5})^{-5/6}}{(1 + 0.9d_0^2 + 0.62d_0^2\sigma_0^{12/5})^{5/6}}\right] - 1\right)^{-1}, \tag{10}$$

where $\sigma_0^2 = 0.492C_n^2\hat{k}^{7/6}L^{11/6}$ denote the Rytov variance, $d_0 = \sqrt{2\pi D^2/4L\lambda}$, L is the distance between S and R, λ is the operational wavelength, D is the aperture diameter of the receiver,

and C_n^2 is the altitude-dependent index of the refractive structure parameter determining the turbulence strength. Additionally, we presume that C_n^2 is constant during reasonably long transmit bit intervals [56].

Since it represents a variety of models often used in communication systems for a variety of combinations of α and β, the distribution in (8) is general. Thus, as $\alpha \to \infty$, it approximates the well-known Gamma distribution (or alternatively squared Nakagami-m [57]), whereas for $\beta = 1$, it corresponds to the statistics of a squared K-distributed RV, with a PDF given by

$$f_{\gamma_0}(x;\alpha,1,\Omega_0) = \frac{2(\alpha)^{\frac{\alpha+\beta}{2}} x^{\frac{\alpha+\beta}{2}-1}}{\Gamma(\alpha)\Omega_0^{\frac{\alpha+\beta}{2}}} K_{\alpha-1}\left(2\sqrt{\frac{\alpha}{\Omega_0}x}\right), \tag{11}$$

where $K_q(\cdot)$ denotes the q^{th} order of the modified Bessel function of the second kind.

It can then be simplified to the power statistics of the double Rayleigh model, which is often employed in cascade multipath fading channels, with the PDF obtained from [58] for the particular case of α and β:

$$f_{\gamma_0}(x;1,1,\Omega_0) = \frac{2}{\Omega_0} K_0\left(2\sqrt{\frac{x}{\Omega_0}}\right). \tag{12}$$

Now, we obtain the p-th moment of γ_0 as given by [54]:

$$\mathbb{E}[\gamma_0^p] = \xi^{-p} \frac{\Gamma(\alpha+p)\Gamma(\beta+p)}{(\alpha\beta)^p \Gamma(\alpha)\Gamma(\beta)} \tag{13}$$

where $\xi = \frac{\alpha\beta}{\Omega_0}$. Furthermore, [59, Eq. (7)] and [60, Eq. (9.31.5)] can be applied to define the cumulative density function (CDF), expressed as

$$F_{\gamma_0}(x;\alpha,\beta,\Omega_0) = \frac{1}{\Gamma(\alpha)\Gamma(\beta)} G_{1,3}^{2,1}\left(\xi x \middle| \begin{matrix} 1 \\ \alpha,\beta,0 \end{matrix}\right), \tag{14}$$

where $G_{p,q}^{m,n}(.)$ is the Meijer G-function [20, Eq. 9.301].

3.2 Fading statistics of the RF channel

Both the R to D_1 and R to D_2 routes in the RF path are modeled with Nakagami-m distribution and fading severity parameters m_{h_1} and m_{h_2}, respectively. The CDF and PDF of $|h_u|^2$, $u \in \{1, 2\}$ may therefore be expressed as [61]

$$f_{|h_u|^2}(x) = \frac{{\mu_u}^{m_u} e^{-\mu_u x} x^{m_u-1}}{\Gamma(m_u)}, \tag{15a}$$

$$F_{|h_u|^2}(x) = 1 - e^{-\mu_u x} \sum_{s=0}^{m_u-1} \frac{\mu_u^s x^s}{s!}, \tag{15b}$$

where $\mu_u = \frac{m_u}{\lambda_u}$, in which m_u and λ_u represent the integer fading factor and the mean, respectively.

In addition, the scenario $R_2 \geq R_1$ (R_1 and R_2 are the radii of the inner and outer circles, respectively), note that the users are deployed in D_1 and D_2 based on homogeneous poisson point processes. Consequently, NOMA users are characterized as independently and identically distributed (i.i.d.) points in D_1 and D_2, indicated by d_u, $u \in \{1, 2\}$, which carry location information about nearby and distant users, respectively. The d_1 and d_2 probability density

functions (PDFs) are provided by [62]:

$$f_{d_1}(x) = \frac{\partial}{\partial x}\frac{\pi x^2}{\pi R_1^2} = \frac{2x}{R_1^2}, \tag{16}$$

$$f_{d_2}(x) = \frac{\partial}{\partial x}\frac{\pi(x^2 - R_1^2)}{\pi(R_2^2 - R_1^2)} = \frac{2x}{R_2^2 - R_1^2}. \tag{17}$$

4 Outage probability analysis

4.1 Outage probability of D_1

Signal x_1 cannot be received successfully by D_1 when the following cases occur: when R is unable to decode either x_2 or x_1 and when D_1 fails to perform SIC for x_2 and is thus unable to decode x_1.

The outage probabilities in the first and second cases are given by

$$\begin{aligned}\mathcal{P}_{out}^1 &= 1 - \Pr\begin{pmatrix}\gamma_{R,x_2}^{SIC} > \gamma_{th}^2, \gamma_{R,x_1}^{ipSIC} > \gamma_{th}^1, \\ \gamma_{1,x_2}^{SIC} > \gamma_{th}^2, \gamma_{1,x_1}^{ipSIC} > \gamma_{th}^1\end{pmatrix} \\ &= 1 - \mathcal{I}_1\mathcal{I}_2,\end{aligned} \tag{18}$$

where $\mathcal{I}_1 = \Pr(\gamma_{R,x_2}^{SIC} > \gamma_{th}^2, \gamma_{R,x_1}^{ipSIC} > \gamma_{th}^1)$, $\mathcal{I}_2 = \Pr(\gamma_{1,x_2}^{SIC} > \gamma_{th}^2, \gamma_{1,x_1}^{ipSIC} > \gamma_{th}^1)$ and $\gamma_{th}^u = 2^{2R_{th}^u} - 1$, with R_{th}^u being the target rate at of D_u, $\forall u \in \{1, 2\}$.

The closed-form formulation of $\mathcal{P}_{out}^1$ is provided in Proposition 1 from (18).

Proposition 1 *The proposed FSO/RF dual-hop relay system's* $\mathcal{P}_{out}^1$ *is calculated from the Eq*:

$$\begin{aligned}\mathcal{P}_{out}^1 &= 1 - 2\sum_{s=0}^{m_1-1}\frac{\mu_1^s\Theta_{\max}^s\gamma(\vartheta, \mu_1\Theta_{\max}R_1^\delta)}{s!R_1^{2\delta}\mu_1^\vartheta\Theta_{\max}^\vartheta} \\ &\times\left(1 - \frac{1}{\Gamma(\alpha)\Gamma(\beta)}G_{1,3}^{2,1}\left(\xi\Theta_{\max}\middle|\begin{matrix}1\\ \alpha, \beta, 0\end{matrix}\right)\right),\end{aligned} \tag{19}$$

where $\Theta_1 = \frac{\gamma_{th}^1}{\rho(a_1 - \gamma a_2\gamma_{th}^1)}$, $\Theta_2 = \frac{\gamma_{th}^2}{\rho(a_2 - a_1\gamma_{th}^2)}$, $\Theta_{\max} = \max(\Theta_1, \Theta_2)$ *and* $\vartheta = \frac{\delta s+2}{\delta}$.

Proof 1 *See* S1 Appendix.

4.2 Outage probability of D_2

Similarly, in the first case, the signals x_1 and x_2 cannot be effectively received by R. Then, in the second case, D_2 fails to decode the signal x_2. The outage probability of D_2 is therefore be calculated as follows:

$$\begin{aligned}\mathcal{P}_{out}^2 &= 1 - \Pr(\gamma_{R,x_2}^{SIC} > \gamma_{th}^2, \gamma_{R,x_1}^{ipSIC} > \gamma_{th}^1) \\ &+\Pr(\gamma_{R,x_2}^{SIC} > \gamma_{th}^2, \gamma_{R,x_1}^{ipSIC} > \gamma_{th}^1)\Pr(\gamma_{2,x_2}^{SIC} < \gamma_{th}^2) \\ &= 1 - \mathcal{I}_1 + \mathcal{I}_1\mathcal{I}_3,\end{aligned} \tag{20}$$

where $\mathcal{I}_3 = \Pr(\gamma_{2,x_2} < \gamma_{th}^2)$.

Proposition 2 gives the closed-form expression of $\mathcal{P}_{out}^2$, derived from (20).

Proposition 2 *The proposed FSO/RF dual-hop relay system's* $\mathcal{P}_{out}^{2}$ *is computed from the Eq*:

$$\begin{aligned}\mathcal{P}_{out}^{2} &= 1-\left[1-\frac{1}{\Gamma(\alpha)\Gamma(\beta)}G_{1,3}^{2,1}\left(\xi\Theta_{\max}\middle|\begin{matrix}1\\ \alpha,\beta,0\end{matrix}\right)\right]\\ &+\left[1-\frac{1}{\Gamma(\alpha)\Gamma(\beta)}G_{1,3}^{2,1}\left(\xi\Theta_{\max}\middle|\begin{matrix}1\\ \alpha,\beta,0\end{matrix}\right)\right]\\ &\times\left\langle 1-\frac{2}{(R_2^2-R_1^2)}\sum_{s=0}^{m_2-1}\frac{\mu_2^s\Theta_2^s}{s!\delta\mu_2^{\vartheta}\Theta_2^{\vartheta}}\right.\\ &\times[\gamma(\vartheta,\mu_2\Theta_2)+\Gamma(\vartheta,\mu_2\Theta_2)\\ &\left.-\gamma(\vartheta,\mu_2\Theta_2R_1^{\delta})-\Gamma(\vartheta,\mu_2\Theta_2R_2^{\delta})]\right\rangle,\end{aligned} \tag{21}$$

where Θ_2, $\Theta_{\max}$, ξ *and* ϑ *are announced previously*.

Proof 2 *See* S2 Appendix.

4.3 High SNR regime

In this section, we examine outages in the high SNR regime, i.e., when $\rho\to\infty$.

From [63, Eq. (18)], the $G_{p,q}^{m,n}(.)$ Meijer G-function is given by the approximation:

$$\begin{aligned}&G_{p,q}^{m,n}\left(z\middle|\begin{matrix}a_1,\ldots,a_n,a_{n=1},\ldots,a_p\\ b_1,\ldots,b_m,b_{m+1},\ldots,b_q\end{matrix}\right)\\ &\approx\sum_{k=1}^{m}\frac{\prod_{j=1,j\neq k}^{m}\Gamma(b_j-b_k)\prod_{j=1}^{n}\Gamma(1-a_j+b_k)}{\prod_{j=n+1}^{p}\Gamma(a_j-b_k)\prod_{j=m+1}^{q}\Gamma(1-b_j+b_k)}z^{b_k}.\end{aligned} \tag{22}$$

Then, we obtain $\mathcal{I}_1^{\infty}$ from:

$$\begin{aligned}\mathcal{I}_1^{\infty} &\approx 1-\frac{1}{\Gamma(\alpha)\Gamma(\beta)}\\ &\times\left[\frac{\Gamma(\beta-\alpha)}{\alpha}(\xi\Theta_{\max})^{\alpha}+\frac{\Gamma(\alpha-\beta)}{\beta}(\xi\Theta_{\max})^{\beta}\right].\end{aligned} \tag{23}$$

When $x\to 0$, the approximate expressions of the CDF for the channel gain $|h_u|^2$, $u\in\{1,2\}$ are given by [64, Eq. (16a)]

$$F_{|h_u|^2}(x)\approx\frac{(\mu_u x)^{m_u}}{m_u!}. \tag{24}$$

Aided by (24), we obtain $\mathcal{I}_2^{\infty}$ and $\mathcal{I}_3^{\infty}$:

$$\begin{aligned}\mathcal{I}_2^{\infty} &= \int_0^{R_1} f_{d_1}(x)\left[1 - F_{|h_1|^2}(\Theta_{\max}x^{\delta})\right]dx \\ &= \frac{2}{R_1^2}\int_0^{R_1} x\left[1 - \frac{(\mu_1\Theta_{\max})^{m_1}x^{m_1\delta}}{m_1!}\right]dx \\ &= 1 - 2\frac{\mu_1^{m_1}\Theta_{\max}^{m_1}R_1^{m_1\delta}}{m_1!(m_1\delta+2)},\end{aligned} \tag{25}$$

and

$$\begin{aligned}\mathcal{I}_3^{\infty} &= \int_{R_1}^{R_2} f_{d_2}(x)[1 - F_{|h_2|^2}(\Theta_2 x^{\delta})]dx \\ &= 1 - \frac{2\mu_2^{m_2}\Theta_2^{m_2}}{m_2!(R_2^2 - R_1^2)}\int_{R_1}^{R_2} x^{\delta m_2+1}dx \\ &= 1 - \frac{2\mu_2^{m_2}\Theta_2^{m_2}}{m_2!(R_2^2 - R_1^2)(\delta m_2+2)}\left[R_2^{\delta m_2+2} - R_1^{\delta m_2+2}\right].\end{aligned} \tag{26}$$

Finally, we obtain the asymptotic outage probabilities of D_1 and D_2 from (27) and (28), respectively:

$$\begin{aligned}\mathcal{P}_{out}^{1,\infty} &= 1 - \left\langle 1 - \frac{1}{\Gamma(\alpha)\Gamma(\beta)}\left[\frac{\Gamma(\beta-\alpha)}{\alpha}(\xi\Theta_{\max})^{\alpha} + \frac{\Gamma(\alpha-\beta)}{\beta}(\xi\Theta_{\max})^{\beta}\right]\right\rangle \\ &\quad \times\left[1 - 2\frac{\mu_1^{m_1}\Theta_{\max}^{m_1}R_1^{m_1\delta}}{m_1!(m_1\delta+2)}\right].\end{aligned} \tag{27}$$

$$\begin{aligned}\mathcal{P}_{out}^{2,\infty} &= 1 - \left\langle 1 - \frac{1}{\Gamma(\alpha)\Gamma(\beta)}\left[\frac{\Gamma(\beta-\alpha)(\xi\Theta_{\max})^{\alpha}}{\alpha} + \frac{\Gamma(\alpha-\beta)(\xi\Theta_{\max})^{\beta}}{\beta}\right]\right\rangle \\ &\quad + \left\langle 1 - \frac{1}{\Gamma(\alpha)\Gamma(\beta)}\left[\frac{\Gamma(\beta-\alpha)(\xi\Theta_{\max})^{\alpha}}{\alpha} + \frac{\Gamma(\alpha-\beta)(\xi\Theta_{\max})^{\beta}}{\beta}\right]\right\rangle \\ &\quad \times\frac{2\mu_2^{m_2}\Theta_2^{m_2}[R_2^{\delta m_2+2} - R_1^{\delta m_2+2}]}{m_2!(R_2^2 - R_1^2)(\delta m_2+2)}.\end{aligned} \tag{28}$$

5 Numerical results

In this section, we evaluate the performance of the derived theoretical expression and also validate it with numerical results. The fading parameters were set to $m = m_{h_0} = m_{h_1} = m_{h_2}$. Table 3 summarizes the main parameters. Furthermore, the corresponding noise power at D_1 and D_2 was computed as $\sigma^2 = N_0 + 10\log(\mathrm{BW}) + \mathrm{NF}$ [dBm] in [65]. The technological advancement of our code resides in the implementation of symbolic computations within Matlab, which facilitated the attainment of highly precise results.

Table 3. Main parameters for the simulations [55, 62].

Parameters	Notation	Values
Power splitting factors	$\{a_1, a_2\}$	{0.1, 0.9}
Target rates decode x_1 and x_2	$\{R_{th}^1, R_{th}^2\}$	{1, 0.5}
Inner circle radius	R_1	50 m
Outer circle radius	R_2	100 m
Path-loss exponent	δ	3
Channel gains	$\{\lambda_1, \lambda_2\}$	{0.1, 0.1}
Fading severity parameter	m	3
Bandwidth	BW	10 [MHz]
Noise figure	NF	10 [dBm]
Thermal noise power density	N_0	−174 [dBm/Hz]
SIC efficiency	χ	0.01
Distance between S and R	L	4000 m
Receiver aperture diameter	D	0.01 m
Operational wavelength	λ	1550 nm
Turbulence strength	C_n^2	$3 \times 10^{-14} \mathrm{m}^{-2/3}$

https://doi.org/10.1371/journal.pone.0315123.t003

Fig 2 illustrates the outage probability of a dual-hop FSO/RF system as a function of the SIC capability, denoted χ, for near users. The outage probability decreases as the value of m increases from 1 to 3 to 5. This trend can be explained by a larger value of m resulting in a larger sequence containing the sum function in Eq (19), leading to a smaller OP when 1 minus

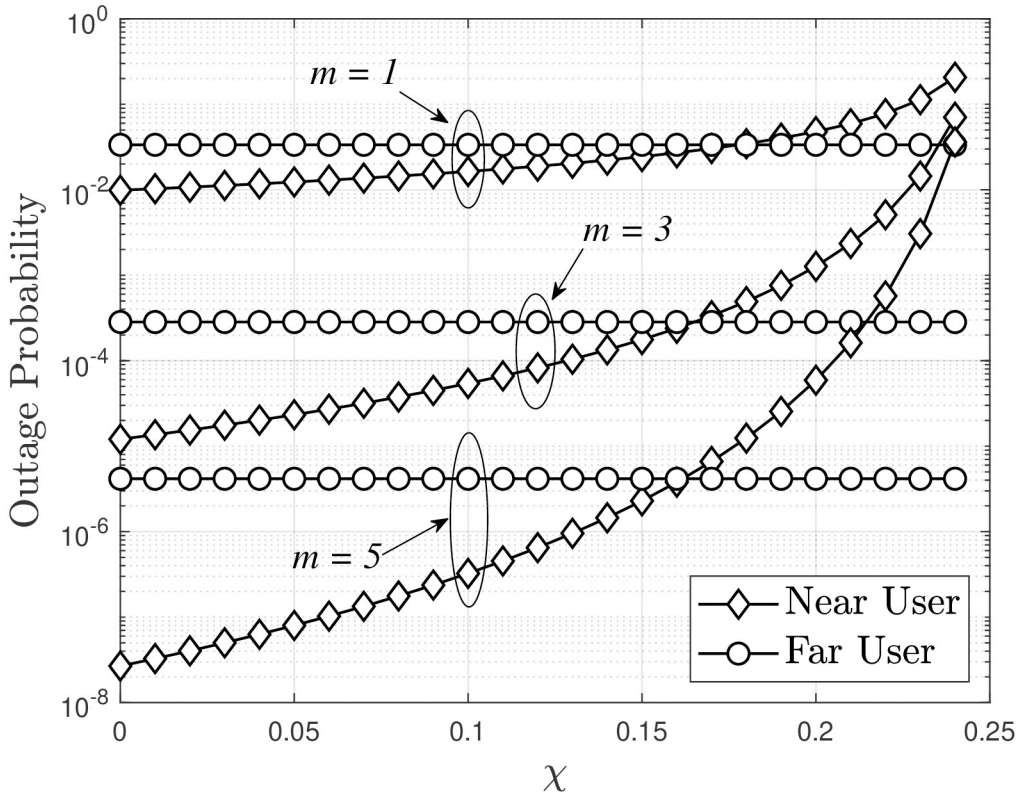

Fig 2. Outage probability of a dual-hop FSO/RF system versus SIC capability χ, with $R_{th}^1 = R_{th}^2 = 0.5$, $a_1 = 0.2$, $a_2 = 0.8$ and $P_S = -10$ [dBm].

https://doi.org/10.1371/journal.pone.0315123.g002

that series is considered. As the SIC capability χ changes from perfect SIC ($\chi = 0$) to $\chi = 0.25$, the OP also varies, reaching its lowest value at $\chi = 0$ and gradually increasing as χ increases. Notably, when χ is approximately 0.24, the OP approaches an asymptotic value for all three cases of m considered. This observation highlights that the more effective the relay's effective interference cancellation capability, the better the system's performance.

In Fig 3, the OP of the system is evaluated as a function of P_S(dBm). It is observed that an increase in P_S(dBm) leads to a decrease in the OP. This is because higher P_S(dBm) values result in higher energy at the relay, which significantly improves the received SINR. In addition, increasing m results in better OP performance, similar to the trend observed in Fig 2. The asymptotic OP of destinations D_1 and D_2, as presented in Eqs (27) and (28), is also accurately simulated in Fig 3. Specifically, for $P_S > -15$ dBm, the asymptotic OP and the actual OP are almost identical.

In addition to increasing m in order to improve OP performance, as observed in Figs 2 and 4 indicates that two users experience different outage performance as the power allocation factor varies. Specifically in this case, the lowest OP for user D_1 occurs when $a_2 = 0.6$, while for user D_2, it occurs when $a_2 = 0.95$. This behavior can be explained by considering that as a_2 is increases, a_1 decreases, leading to an increase in the received SINR at D_2, as indicated by Eq (7). Hence, the OP at the D_2 source always decreases. However, the received SINR at D_1 may increase (based on Eq (5)) or decrease (based on Eq (6)). Therefore, the OP expression in Eq (18) does not show a clear trend of increasing or decreasing, but through simulation and under the condition $a_2 > a_1$, when a_2 increases from 0.6 to 0.95, the OP of near users also increases and converges to an asymptotic value when $a_2 = 0.95$. As a result, as a_2 increases, the

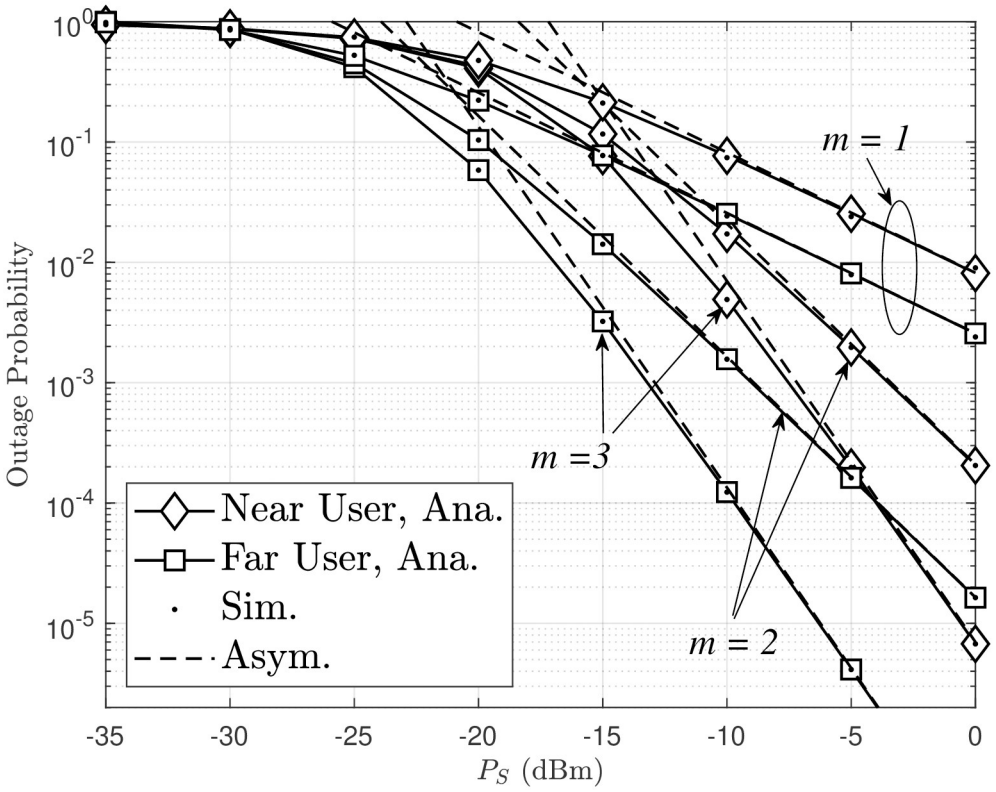

Fig 3. Outage probability of a dual-hop FSO/RF system versus P_S.

https://doi.org/10.1371/journal.pone.0315123.g003

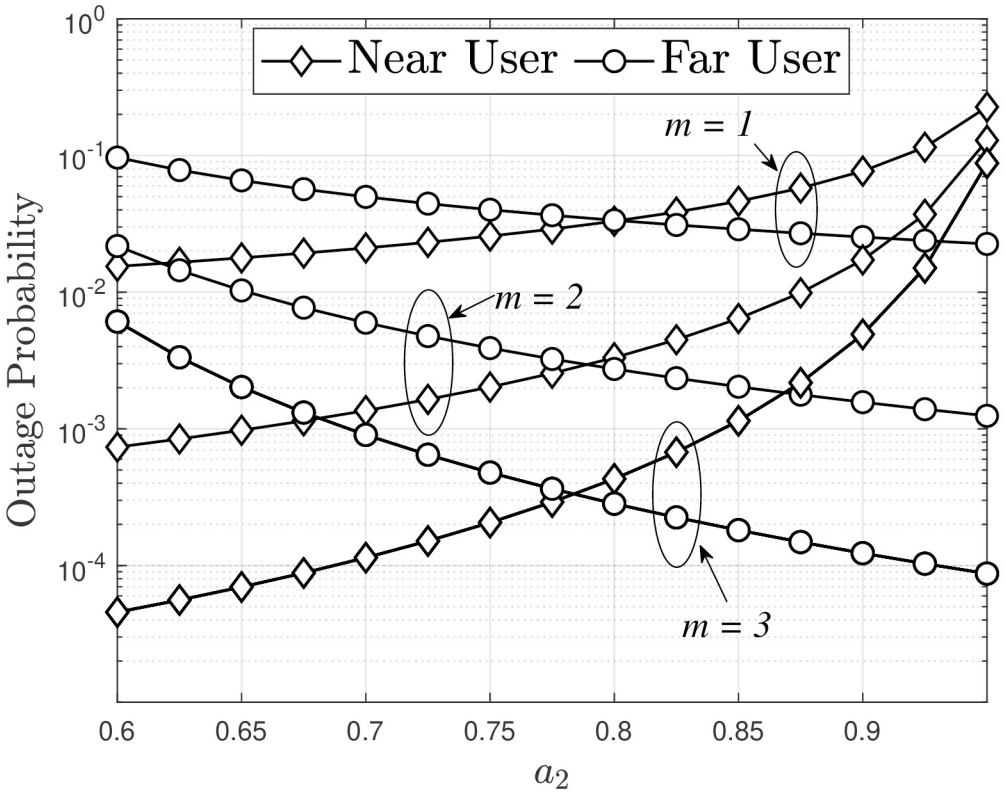

Fig 4. Outage probability versus power allocation factors, with $P_S = -10$ [dBm], $R_{th}^1 = 1$ and $R_{th}^2 = 0.5$.

https://doi.org/10.1371/journal.pone.0315123.g004

far user's OP performance improves while the near user's OP performance deteriorates, and vice versa. To ensure fairness between users, an optimal level of the power allocation factor exists; this is achieved when $a_2 \approx 0.7$ (corresponding to $a_1 = 0.3$), resulting in nearly equal OP performance for both near and far users.

Fig 5 illustrates the outage probability of the model when compared to $R_{th}^1 = R_{th}^2$, with $\rho =$ 30 [dB], $a_1 = 0.05$ and $a_2 = 0.95$. As $R_{th}^1 = R_{th}^2$ increases, the user's OP efficiency decreases, as explained by Eqs (18) and (20). In addition, the OP performance of distant users is better than that of proximity users. This is because, with a power allocation factor $a_2 = 0.95$, distant users achieve their best OP performance (as previously indicated in Fig 4). In Fig 6 presents the outage probability versus PS (in dBm) for different scenarios in a wireless communication system, showing that the NOMA scheme achieves better performance for both near and far users compared to the conventional OMA, with asymptotic and simulated results depicted by dashed and solid lines, respectively, demonstrating the superior robustness of NOMA, especially at higher transmit power levels.

Fig 7 shows the outage probability of FSO and FSO-RF links at both near and far users as a function of P_S(dBm), with simulated (solid lines) and asymptotic (dashed lines) results indicating better performance at higher power levels. the figure highlights that both user distance and link type (FSO or FSO-RF) significantly impact outage probability, with the near-user FSO link providing the best reliability. Increasing transmit power P_S reduces the outage probability across all configurations, the performance of users for FSO-RF NOMA network is better than FSO NOMA network.

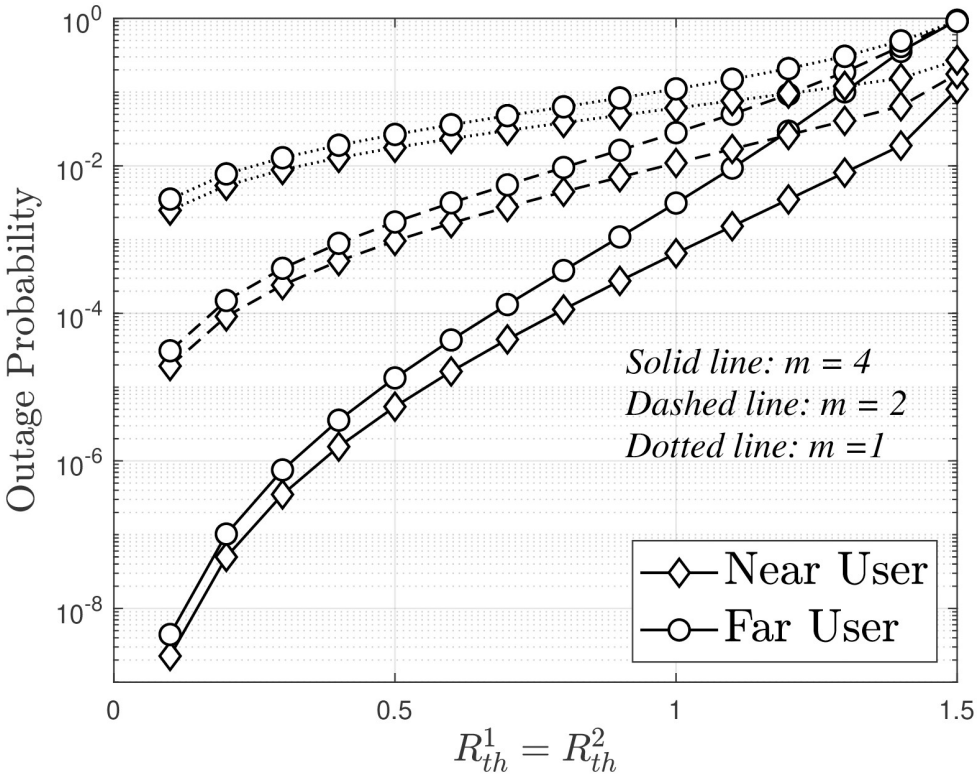

Fig 5. Outage probability versus $R_{ih}^{1} = R_{ih}^{2}$, with $P_S = -10$ [dBm], $a_1 = 0.12$ and $a_2 = 0.88$.

https://doi.org/10.1371/journal.pone.0315123.g005

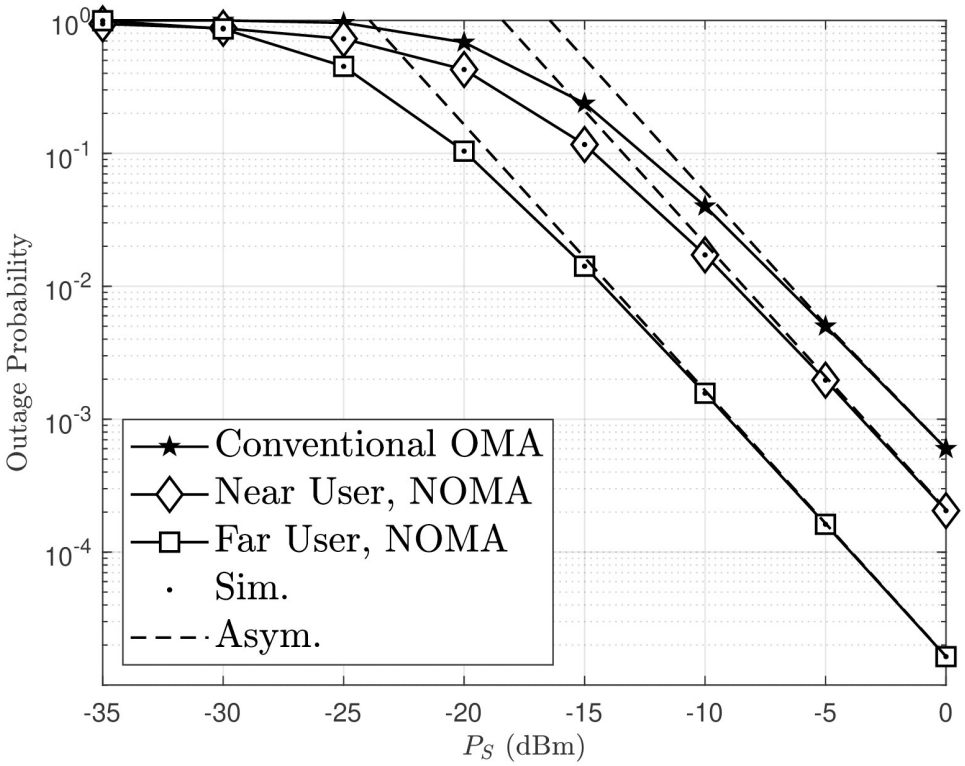

Fig 6. Outage probability versus P_S in NOMA and OMA, with $m = 2$, $a_1 = 0.1$ and $a_2 = 0.9$.

https://doi.org/10.1371/journal.pone.0315123.g006

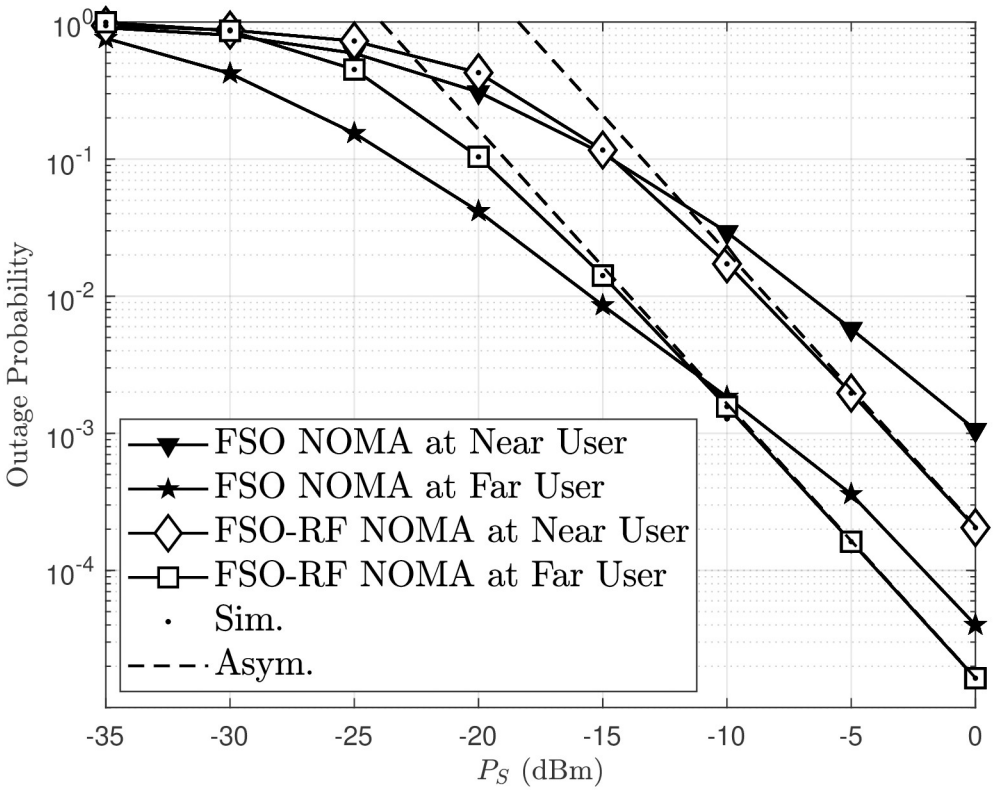

Fig 7. Outage probability versus P_S in FSO link and FSO-RF link, with $m = 2$ and $\chi = 0.01$.

https://doi.org/10.1371/journal.pone.0315123.g007

6 Conclusion

This paper provides a performance analysis of a dual-hop mixed RF-FSO system integrated with NOMA communications technology. Using DF relaying, the relay R employs successive interference cancellation, where the FSO link from the source to the relay follows a double Gamma distribution, and the RF link from the relay to multiple users follow the Nakagami-*m* distribution. Based on this system model, we analyzed the outage probability. Our results demonstrate that SIC has a clear effect on OP performance; specifically the greater the SIC capability, the better the system's performance. We also varied the Nakagami-*m* channel parameters to examine their effect on system performance. The results indicate that increasing the *m* value enhances system performance. The power allocation factors also notably affect OP performance for both near and far users. A higher power allocation factor for far users results in improved OP efficiency for those users but reduced OP efficiency for near users, and vice versa. Consequently, there is a trade-off in OP performance between users. However, an optimal level of the power allocation factor exists that ensures fairness between users. The system's performance also depends on other system parameters. An analysis of these parameters provides insight into optimizing the design and operation of dual-hop mixed RF-FSO systems with NOMA technology.

Supporting information

S1 Appendix. Proof of Proposition 1.
(PDF)

S2 Appendix. Proof of Proposition 2.
(PDF)

S1 File.
(RAR)

Author Contributions

Data curation: Thu-Ha Thi Pham.

Formal analysis: Tran Cong Hung.

Funding acquisition: Miroslav Voznak.

Investigation: Tran Cong Hung, Pham Ngoc Son, Miroslav Voznak.

Methodology: Tran Cong Hung, N. H. K. Nhan.

Software: Tan N. Nguyen, Anh-Tu Le, Thu-Ha Thi Pham.

Validation: Tan N. Nguyen.

Writing – review & editing: N. H. K. Nhan, Pham Ngoc Son.

References

1. Fazio P., Sottile C., Santamaria A. F., Tropea M. Vehicular networking enhancement and multi-channel routing optimization, based on multi-objective metric and minimum spanning tree. Advances in Electrical and Electronic Engineering 2013; 11(5):349–356. https://doi.org/10.15598/aeee.v11i5.903
2. Fazio, P., Tropea, M., Veltri, F., Marano, S. A new routing protocol for interference and path-length minimization in vehicular networks. In 2012 IEEE 75th Vehicular Technology Conference (VTC Spring); 2012 May;1-5; Yokohama, Japan: IEEE.
3. Khalighi M. A., Uysal M. Survey on free space optical communication: A communication theory perspective. IEEE communications surveys & tutorials 2013; 16(4):2231–2258. https://doi.org/10.1109/COMST.2014.2329501
4. Anbarasi K., Hemanth C., Sangeetha R. G. A review on channel models in free space optical communication systems. Optics & Laser Technology 2017; 97:161–171. https://doi.org/10.1016/j.optlastec.2017.06.018
5. Garlinska M., Pregowska A., Gutowska I., Osial M., Szczepanski J. Experimental study of the free space optics communication system operating in the 8–12 μm spectral range. Electronics 2021; 10 (8):875. https://doi.org/10.3390/electronics10080875
6. Wang Y., Xu, et al. Performance analysis of an adaptive optics system for free-space optics communication through atmospheric turbulence. Scientific reports 2018; 8(1):1124. https://doi.org/10.1038/s41598-018-19559-9 PMID: 29348561
7. Ullah Rahat, et al. High-capacity free space optics-based passive optical network for 5g front-haul deployment. Photonics 2023; 10(10):1073. https://doi.org/10.3390/photonics10101073
8. Xu G., Song Z. Effects of solar scintillation on deep space communications: challenges and prediction techniques. IEEE Wireless Communications 2019; 26(2):10–16. https://doi.org/10.1109/MWC.2019.1800271
9. Kaushal H., Kaddoum G Optical communication in space: Challenges and mitigation techniques. IEEE communications surveys & tutorials 2016; 19(1):57–96. https://doi.org/10.1109/COMST.2016.2603518
10. Ullah Rahat, et al. Optimization and analysis of Spectral/Spatial optical code division multiple access passive optical network. AEU-International Journal of Electronics and Communications 2024; 175:155084.
11. Nguyen T. N., Duy T. T., Luu G. T., Tran P. T., Vozňák M. Energy harvesting-based spectrum access with incremental cooperation, relay selection and hardware noises. Radioengineering 2017; 26(1):240–250. https://doi.org/10.13164/re.2017.0240
12. Liang H., Gao C., Li Y., Miao M., Li X. Performance analysis of mixed MISO RF/SIMO FSO relaying systems. Optics Communications 2021; 478:126344. https://doi.org/10.1016/j.optcom.2020.126344

13. Petkovic M. I., Ansari I. S., Djordjevic G. T., Qaraqe K. A. Error rate and ergodic capacity of RF-FSO system with partial relay selection in the presence of pointing errors. Optics Communications 2019; 438:118–125. https://doi.org/10.1016/j.optcom.2019.01.028

14. Zedini E., Ansari I. S., Alouini M. S. Performance analysis of mixed Nakagami-*m* and Gamma–Gamma dual-hop FSO transmission systems. IEEE Photonics Journal 2014; 7(1):1–20. https://doi.org/10.1109/JPHOT.2014.2381657

15. Jamali M. V., Mahdavifar H. Uplink non-orthogonal multiple access over mixed RF-FSO systems. IEEE Transactions on Wireless Communications 2020; 19(5):3558–3574. https://doi.org/10.1109/TWC.2020.2974947

16. Yang L., Liu T., Chen J., Alouini M. S. Physical-Layer Security for Mixed η–μ and $\mathcal{M}$-Distribution Dual-Hop RF/FSO Systems. IEEE transactions on vehicular technology 2018; 67(12):12427–12431. https://doi.org/10.1109/TVT.2018.2877136

17. Wang Z., Shi W., Liu W. Performance analysis of mixed RF/FSO system with spatial diversity. Optics Communications 2019; 443:230–237. https://doi.org/10.1016/j.optcom.2019.03.040

18. Yi X., Shen C., Yue P., Wang Y., Ao Q. Performance of decode-and-forward mixed RF/FSO system over κ—μ shadowed and exponentiated Weibull fading. Optics Communications 2019; 439:103–111. https://doi.org/10.1016/j.optcom.2019.01.003

19. Balti E., Guizani M. Mixed RF/FSO cooperative relaying systems with co-channel interference. IEEE Transactions on Communications 2018; 66(9):4014–4027. https://doi.org/10.1109/TCOMM.2018.2818697

20. Upadhya A., Gupta J., Dwivedi V. K., Alouini M. S. Impact of RF I/Q imbalance on interference-limited mixed RF/FSO TWR systems with non-zero boresight error. IEEE Wireless Communications Letters 2020; 10(2):416–420. https://doi.org/10.1109/LWC.2020.3033528

21. Pham X. N., et al. Enhancing data rate and energy efficiency of NOMA systems using reconfigurable intelligent surfaces for millimeter-wave communications. Digital Signal Processing 2024; 151:104553. https://doi.org/10.1016/j.dsp.2024.104553

22. Vo D. T., Nguyen T. N., Le A. T., Phan V. D., Voznak M. Holographic Reconfigurable Intelligent Surface-Aided Downlink NOMA IoT Networks in Short-Packet Communication. IEEE Access 2024; 12:65266–65277.

23. Le AT, Hieu TD, Nguyen TN, Le TL, Nguyen SQ, Voznak M. Physical layer security analysis for RIS-aided NOMA systems with non-colluding eavesdroppers. Computer Communications. 2024; 219:194–203. https://doi.org/10.1016/j.comcom.2024.03.011

24. Le AT, Tran DH, Le CB, Tin PT, Nguyen TN, Ding Z, et al. Power Beacon and NOMA-Assisted Cooperative IoT Networks With Co-Channel Interference: Performance Analysis and Deep Learning Evaluation. IEEE Transactions on Mobile Computing. 2024; 23(6):7270–7283. https://doi.org/10.1109/TMC.2023.3333764

25. Ma Yiming, et al. NOMA security scheme based on constellation camouflage and selective mapping. Optics Letters. 2023; 48(15):4101–4104. https://doi.org/10.1364/OL.493540 PMID: 37527128

26. Timotheou S, Krikidis I. Fairness for Non-Orthogonal Multiple Access in 5G Systems. IEEE Signal Processing Letters. 2015; 22(10):1647–1651 https://doi.org/10.1109/LSP.2015.2417119

27. Ding Z, Lei X, Karagiannidis GK, Schober R, Yuan J, Bhargava VK. A Survey on Non-Orthogonal Multiple Access for 5G Networks: Research Challenges and Future Trends. IEEE Journal on Selected Areas in Communications. 2017; 35(10):2181–2195. https://doi.org/10.1109/JSAC.2017.2725519

28. Rose K, Eldridge S, Chapin L. The internet of things: An overview. The internet society (ISOC). 2015; 80(15):1–53.

29. Li S, Xu LD, Zhao S. The internet of things: a survey. Information systems frontiers. 2015; 17:243–259. https://doi.org/10.1007/s10796-014-9492-7

30. Hu L, et al. Cooperative Jamming for Physical Layer Security Enhancement in Internet of Things. IEEE Internet of Things Journal. 2018; 5(1):219–228. https://doi.org/10.1109/JIOT.2017.2778185

31. Rappaport TS. Wireless Communications: Principles and Practice. Prentice Hall; 2002.

32. Zhang L, et al. Layered-Division- Multiplexing: Theory and Practice. IEEE Transactions on Broadcasting. 2016; 62(1):216–232. https://doi.org/10.1109/TBC.2015.2505408

33. Qi T, Feng W, Wang Y. Outage performance of non-orthogonal multiple access based unmanned aerial vehicles satellite networks. China Communications. 2018; 15(5):1–8. https://doi.org/10.1109/CC.2018.8387982

34. Sohail MF, Leow CY, Won S. Non-Orthogonal Multiple Access for Unmanned Aerial Vehicle Assisted Communication. IEEE Access. 2018; 6:22716–22727. https://doi.org/10.1109/ACCESS.2018.2826650

35. Yan X, et al. The Application of Power-Domain Non-Orthogonal Multiple Access in Satellite Communication Networks. IEEE Access. 2019; 7:63531–63539. https://doi.org/10.1109/ACCESS.2019.2917060

36. Nguyen NT, Nguyen HN, Nguyen NL, Le AT, Nguyen TN, Voznak M. Performance Analysis of NOMA-Based Hybrid Satellite-Terrestrial Relay System Using mmWave Technology. IEEE Access. 2023; 11:10696–10707. https://doi.org/10.1109/ACCESS.2023.3238335

37. Cheng Y, Li KH, Liu Y, Teh KC, Karagiannidis GK. Non-Orthogonal Multiple Access (NOMA) With Multiple Intelligent Reflecting Surfaces. IEEE Transactions on Wireless Communications. 2021; 20 (11):7184–7195. https://doi.org/10.1109/TWC.2021.3081423

38. Phu LS, et al. Improving the Capacity of NOMA Network Using Multiple Aerial Intelligent Reflecting Surfaces. IEEE Access. 2023; 11:107958–107971. https://doi.org/10.1109/ACCESS.2023.3319675

39. Najafi M, Jamali V, Diamantoulakis PD, Karagiannidis GK, Schober R. Non- orthogonal multiple access for FSO backhauling. In: 2018 IEEE Wireless Communications and Networking Conference (WCNC); 2018. p. 1–6.

40. Li R, Dang A. Performance analysis of non-orthogonal multiple access in free space optical communication system. arXiv preprint arXiv:170706571. 2017;

41. Lei X, Yang L, Zhang J, Li G, Chen J. LAP-Based FSO-RF Cooperative NOMA Systems. In: 2020 IEEE 92nd Vehicular Technology Conference; 2020. p. 1–5.

42. Jamali MV, Mahdavifar H. Uplink Non-Orthogonal Multiple Access Over Mixed RF-FSO Systems. IEEE Transactions on Wireless Communications. 2020; 19(5):3558–3574. https://doi.org/10.1109/TWC.2020.2974947

43. Ben Halima N, Boujemaa H. Optimal power allocation and harvesting duration for mixed RF/FSO using non orthogonal multiple access. Optical and Quantum Electronics. 2020; 52(10):442. https://doi.org/10.1007/s11082-020-02560-w

44. Li R, Chen T, Fan L, Dang A. Performance analysis of a multiuser dual-hop amplify- and-forward relay system with FSO/RF links. Journal of Optical Communications and Networking. 2019; 11(7):362–370. https://doi.org/10.1364/JOCN.11.000362

45. Nguyen ND, Le AT. Employing Non-Orthogonal Multiple Access for A Dual-Hop Relaying System With FSO/RF Links. In: 2021 10th International Conference on Information and Automation for Sustainability (ICIAfS); 2021. p. 346–351.

46. Zhuang Y, Zhang J. Secrecy performance analysis for a NOMA based FSO-RF system with imperfect CSI. Journal of Optical Communications and Networking. 2022; 14(7):500–510. https://doi.org/10.1364/JOCN.454367

47. Samir A, Elsayed M, El-Banna AAA, Shafique Ansari I, Rabie K, ElHalawany BM. Performance analysis of dual-hop hybrid RF-UOWC NOMA systems. Sensors. 2022; 22(12):4521. https://doi.org/10.3390/s22124521 PMID: 35746302

48. Zhang J, Zhang L, Pan G. Outage Performance for NOMA-Based FSO-RF Systems With a Dual Energy Harvesting Mode. IEEE Internet of Things Journal. 2023; 10(18):16076–16086. https://doi.org/10.1109/JIOT.2023.3267136

49. Zhang L, Zhang J, Hu N, Li X, Pan G. Outage Performance for NOMA- Based FSO-RF Systems With Transmit Antenna Selection and Nonlinear Energy Harvesting. IEEE Internet of Things Journal. 2023; 10(7):6491–6506. https://doi.org/10.1109/JIOT.2022.3227043

50. Kumar R, Shukla MK, Kumar V, Tripathi R. Dual-Hop Mixed FSO-RF Wireless Powered Relaying System: Performance Analysis With Nonlinear Energy Harvest- ing. IEEE Transactions on Green Communications and Networking. 2024; p. 1–1. https://doi.org/10.1109/TGCN.2024.3482866

51. Zhou J, Wang R, Shihada B, Alouini MS. End-to-End Uplink Perfor- mance Analysis of Satellite-Based IoT Networks: A Stochastic Geometry Ap- proach. IEEE Open Journal of the Communications Society. 2024; 5:4036–4045. https://doi.org/10.1109/OJCOMS.2024.3422110

52. Sun Q, Hu Q, Wu Y, Chen X, Zhang J, L´opez-Ben´ıtez M. Performance Analysis of Mixed FSO/RF System for Satellite-Terrestrial Relay Network. IEEE Transactions on Vehicular Technology. 2024; 73 (8):11378–11393. https://doi.org/10.1109/TVT.2024.3373653

53. Hoang TM, Nguyen BC, Dung LT, Kim T. Outage Performance of Multi-Antenna Mobile UAV-Assisted NOMA Relay Systems Over Nakagami-m Fading Channels. IEEE Access. 2020; 8:215033–215043. https://doi.org/10.1109/ACCESS.2020.3041311

54. Chatzidiamantis ND, Karagiannidis GK. On the Distribution of the Sum of Gamma-Gamma Variates and Applications in RF and Optical Wireless Com- munications. IEEE Transactions on Communications. 2011; 59(5):1298–1308. https://doi.org/10.1109/TCOMM.2011.020811.090205

55. Zhang J, Dai L, Zhang Y, Wang Z. Unified Performance Analysis of Mixed Radio Frequency/Free-Space Optical Dual-Hop Transmission Systems. Journal of Lightwave Technology. 2015; 33(11):2286–2293. https://doi.org/10.1109/JLT.2015.2409570

56. Navidpour SM, Uysal M, Kavehrad M. BER Performance of Free-Space Optical Transmission with Spatial Diversity. IEEE Transactions on Wireless Communications. 2007; 6(8):2813–2819. https://doi.org/10.1109/TWC.2007.06109

57. NAKAGAMI M. The m-Distribution—A General Formula of Intensity Distribution of Rapid Fading. In: HOFFMAN WC, editor. Statistical Methods in Radio Wave Propagation. Pergamon; 1960. p. 3–36.

58. Uysal M. Diversity analysis of space-time coding in cascaded Rayleigh fading channels. IEEE Communications Letters. 2006; 10(3):165–167. https://doi.org/10.1109/LCOMM.2006.1603372

59. Tsiftsis T. Performance of heterodyne wireless optical communication systems over gamma-gamma atmospheric turbulence channels. Electronics Letters. 2008; 44(5):1. https://doi.org/10.1049/el:20083028

60. Gradshteyn IS, Ryzhik IM. Table of integrals, series, and products. Academic press; 2014.

61. Do DT, Le CB, Vahid A, Mumtaz S. Antenna Selection and Device Grouping for Spectrum-Efficient UAV-Assisted IoT Systems. IEEE Internet of Things Journal. 2023; 10(9):8014–8030. https://doi.org/10.1109/JIOT.2022.3229592

62. Zhao B, Zhang C, Yi W, Liu Y. Ergodic Rate Analysis of STAR-RIS Aided NOMA Systems. IEEE Communications Letters. 2022; 26(10):2297–2301. https://doi.org/10.1109/LCOMM.2022.3194363

63. Lei X, Yang L, Zhang J, Li G, Chen J. LAP-Based FSO-RF Cooperative NOMA Systems. In: 2020 IEEE 92nd Vehicular Technology Conference; 2020. p. 1–5.

64. Dao TTT, Nguyen SQ, Nhung-Nguyen H, Nguyen PX, Kim YH. Performance Evaluation of Downlink Multiple Users NOMA-Enable UAV-Aided Communication Systems Over Nakagami-m Fading Environments. IEEE Access. 2021; 9:151641–151653. https://doi.org/10.1109/ACCESS.2021.3124017

65. Do TN, Kaddoum G, Nguyen TL, da Costa DB, Haas ZJ. Multi- RIS-Aided Wireless Systems: Statistical Characterization and Performance Analysis. IEEE Transactions on Communications. 2021; 69 (12):8641–8658. https://doi.org/10.1109/TCOMM.2021.3117599